THE JOURNAL OF PHYSICAL CHEMISTRY B

ARTICLE

pubs.acs.org/JPCB

Hydration-Determined Orientational Preferences in Aromatic Association from Benzene Dimer Free Energy Volumes

M. Riedaa Gamieldien, Johan Strümpfer, and Kevin J. Naidoo*

Scientific Computing Research Unit and Department of Chemistry, University of Cape Town, Rondebosch 7701, South Africa

ABSTRACT: In this study of the thermodynamics of benzene association in water, we show that although the potential energy and enthalpy play an important role in the association of benzene dimers, they do not determine the relative orientation of these molecules on close contact in solution. We observe a large variation in the configurations that contribute to the vacuum (i.e., solvent-free) minimum free energy wells of the benzene contact pair. In water, fewer and smaller minimum free energy wells are observed. On examination, we find that fewer close contact configurations of benzene dimers populate these wells and that they are more energetically distinct from each other (compared with the vacuum case). The edge-over-edge configuration is most likely in solution and appears to evolve from the entropically favored side-by-side solvent shared configuration. Therefore, the relative orientation of the benzene molecules (i.e., parallel displaced, T-shaped, etc.) on association is a result of maximizing the contribution of the benzene−benzene entropy of association, to the solution free energy.

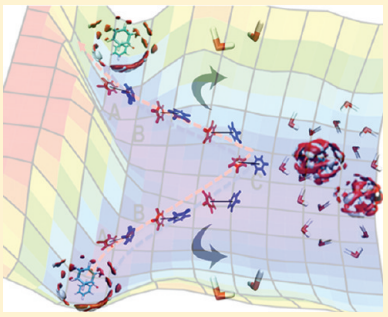

INTRODUCTION

Molecular association between aromatic molecules is at the heart of many important biochemical processes, such as cellular communication and transport,[1] protein folding,[2−4] the mechanism of crystallization,[5] and liquid crystal phases.[6] The particular case of two benzene molecules associating is often used as a central narrative for interior hydrophobic interactions in globular proteins that are responsible for their overall fold, $\pi-\pi$ interactions that help to stabilize base pair stacking in DNA,[7] and that inform the packing of organic crystals and liquid crystalline materials.[6] In all of these important phenomena, it is striking that the aromatic interactions exhibit a strong orientational bias.

The benzene dimer is weakly associating[8−10] and has been the subject of considerable study because of its simplicity and its effectiveness as a model for complex aromatic interactions.[8−11] The geometry of an aromatic pair of molecules may be reduced to four variables that describe the relative distance and orientation of each molecule. In the case of the benzene dimer, we use the vectors normal to each benzene plane and the center of mass of each benzene molecule. The four orientational parameters are then defined (Scheme 1) as the distance of the interconnecting vector between the two benzene centers (r), the angle between each benzene normal vector and interconnecting vector (θ_1, θ_2) and the relative angle between these vectors (ϕ). Using these parameters, we are able to distinguish between previously identified minimum energy configurations that are sandwich (S), T-shaped (T), V-shaped (V), bent T-shaped (BT), side-by-side (SbS), and parallel displaced (PD) (Scheme 1).

Gräfenstein and Cremer comprehensively mapped out the potential energy surface (PES) of the benzene dimer employing a quasi-self-consistent field dispersion-corrected density functional theory formalism (QSCF-DC-DFT).[12] They distinguished among minimum PD and T configurations by specifying when the H−C···C−H fragment of the upper benzene was located exactly over the H−C···C−H fragment of the lower benzene (AoA) or whether it had an atom-over-bond (AoB) or bond-over-bond (BoB) arrangement. In addition, they specified when the benzene rings where edge-over-plane (EoP) and edge-over-edge (EoE). This led to the identification of 16 stationary points on the surface that, when ignoring the relative orientation of the benzene C_6 symmetry, can be conflated to correspond to the S(4), PD(4), B(2), T(5), and SbS(1) geometries.

Here, our interests are focused on macromolecular conformations that are driven by the thermodynamics of hydrophobic association of aromatic groups. It is for this reason that we seek to understand the effect of water on the relative orientation of benzene molecular pairs. To this end, we present a converged multidimensional free-energy volume $W(r, \theta_1, \theta_2, \phi)$ for two benzene molecules in vacuum and water. These free energy volumes are highly informative because they produce not only relative stationary points that correspond to ab initio values but also the configurational pathways linking these favored geometries.

COMPUTATIONAL METHODS

All simulations were performed using our modified version of CHARMM 33b2[13] that incorporates our previously developed Free Energy from Adaptive Reaction Coordinate Forces (FEARCF).[14,15] The FEARCF method was applied to the four-dimensional

Received: August 11, 2011
Revised: November 4, 2011
Published: November 22, 2011

Scheme 1. (a) The Reaction Coordinate Definitions in the Centre and the Various Benzene Dimer Configurations Using Gräfenstein and Cremer Nomenclature and (b) Values above the Configuration Names Corresponding to the r, θ_1, θ_2, ϕ Values for Examples of the Various Configurations

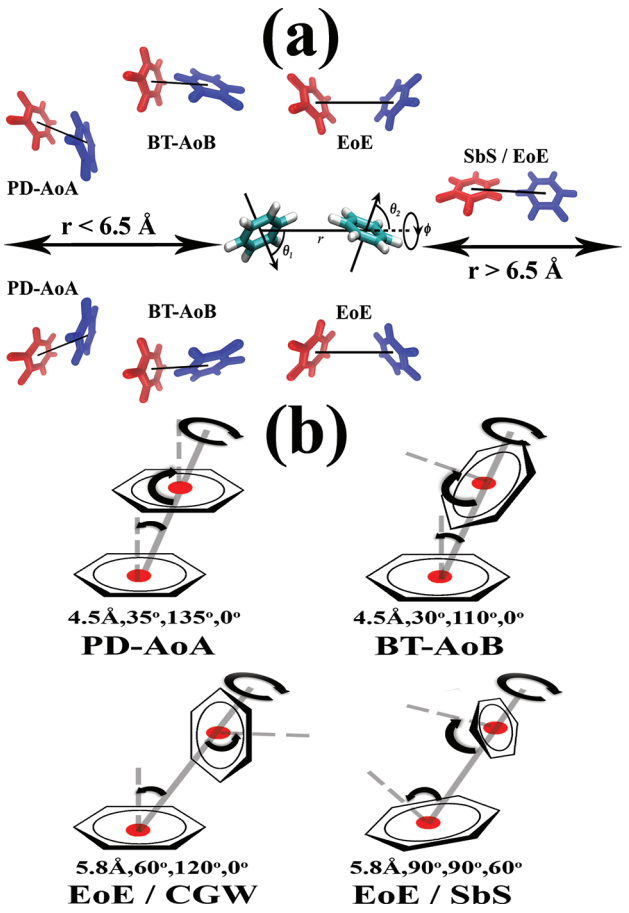

reaction coordinate, ξ, space comprising four independent reaction coordinates: $\xi = (\xi_1 = r, \xi_2 = \theta_1, \xi_3 = \theta_2, \xi_4 = \phi)$. The free energy was deconvoluted into an entropy and energy of association using a "finite difference" method.[16,17]

The calculations of two-dimensional ($W(r, \theta_1)$ and $W(r, \phi)$ for $r \leq 10.0$ Å; $W(\theta_1, \phi)$ and $W(\theta_1, \theta_2)$) and three-dimensional ($W(r, \theta_1, \phi)$, $W(\theta_1, \theta_2, \phi)$) Boltzmann averaged plots were produced to identify configurations from the $W(r, \theta_1, \theta_2, \phi)$ volume taking into account that there can be significant loss of information when reducing the dimensionality of the free energy surfaces.[18]

THE FEARCF METHOD APPLIED TO AROMATIC ASSOCIATION

The FEARCF method is a flat histogram method.[14,19] The reaction coordinate, ξ, space is a discretized four-dimensional grid in which there are four independent reaction coordinates: $\xi = (\xi_1 = r, \xi_2 = \theta_1, \xi_3 = \theta_2, \xi_4 = \phi)$. The sampling frequency for a bin site is recorded for each simulation. The population of this grid represents a running tally of the reaction coordinate probability density, derived from the history of simulations to that point. It is used as input for a multidimensional interpolation from which the reaction coordinate driving forces are calculated. These forces are applied to all atoms used in the reaction coordinate definition to drive the next iteration's trajectory away from previously sampled volumes. The entire reaction coordinate space is equally sampled when the driving forces are derived from the true potential of mean force (PMF). The forces are applied on Cartesian coordinates, and therefore, the PMF does not need a Jacobian correction.[20−23]

The system Hamiltonian is modified by adding the driving potential, $V(\xi)$, derived from the population density of the sampled volume, to the unbiased Hamiltonian, H^0,

$$H(\xi) = H^0 + V(\xi) \tag{1}$$

The biased Hamiltonian $H(\xi)$ is then used in the simulation instead of H^0 and so generates a biased probability distribution of sampled coordinates $P'(\xi)$. This $P'(\xi)$ can then be converted to an unbiased probability distribution by accounting for the driving potential as follows:

$$P'(\xi) = CP'(\xi) \exp\left(\frac{V(\xi)}{k_B T}\right) \tag{2}$$

where C is the normalization constant, k_B is the Boltzmann constant, and T is the temperature of the system. The PMF, $W(\xi)$, is then calculated from the probability distribution of the reaction coordinate assembled from the sampling of all trajectories to that point and is given as

$$W(\xi) = -k_B T \log P(\xi) \tag{3}$$

At each step of the simulation, the driving forces for ξ_i are applied to the atoms involved in the definition of the molecular vectors (for example, as shown in Scheme 1). For four-dimensional surfaces, these are

$$F(\xi) = -\sum_i \frac{\partial V(\xi)}{\partial \xi_i} \tag{4}$$

The force arising from the driving potential is calculated by treating the molecules, which were used in the reaction coordinates definition, as rigid bodies. This ensures that during the simulation, the atoms within each of the benzenes do not move apart and deform due to differing accelerations that arise from the driving potential. Consequently, when the resultant acceleration for a benzene molecule is calculated as a whole, the forces on the atoms are determined such that they experience the same resultant acceleration.

For the first FEARCF iteration, $V(\xi) = 0$, which then evolves progressively along subsequent iterations to eventually mirror $W(\xi)$. To achieve this, each of the iterations consisted of several sets of relatively short simulations (100 ps each), which were initiated from configurations of dimers that occupy significantly different points in reaction coordinate and momentum space. This was followed by an increase in the simulation times (1 ns) to reach convergence (sampling ratio for configurations of 1:10 for most probable:least probable were set as the minimum criteria).

The vacuum FEARCF simulations were carried out using the velocity−Verlet2 (vv2) integrator with a time step of 1 fs,[24] and the temperature was maintained at 298.15 K using the TPCONTROL method (based on the Nose−Hoover thermostat) with TAU set at 0.1.[24] Nonbonded cutoffs of 10, 12, and 14 Å with potential and force switching functions were used. A harmonic

dx.doi.org/10.1021/jp2077159 |J. Phys. Chem. B 2012, 116, 324–331

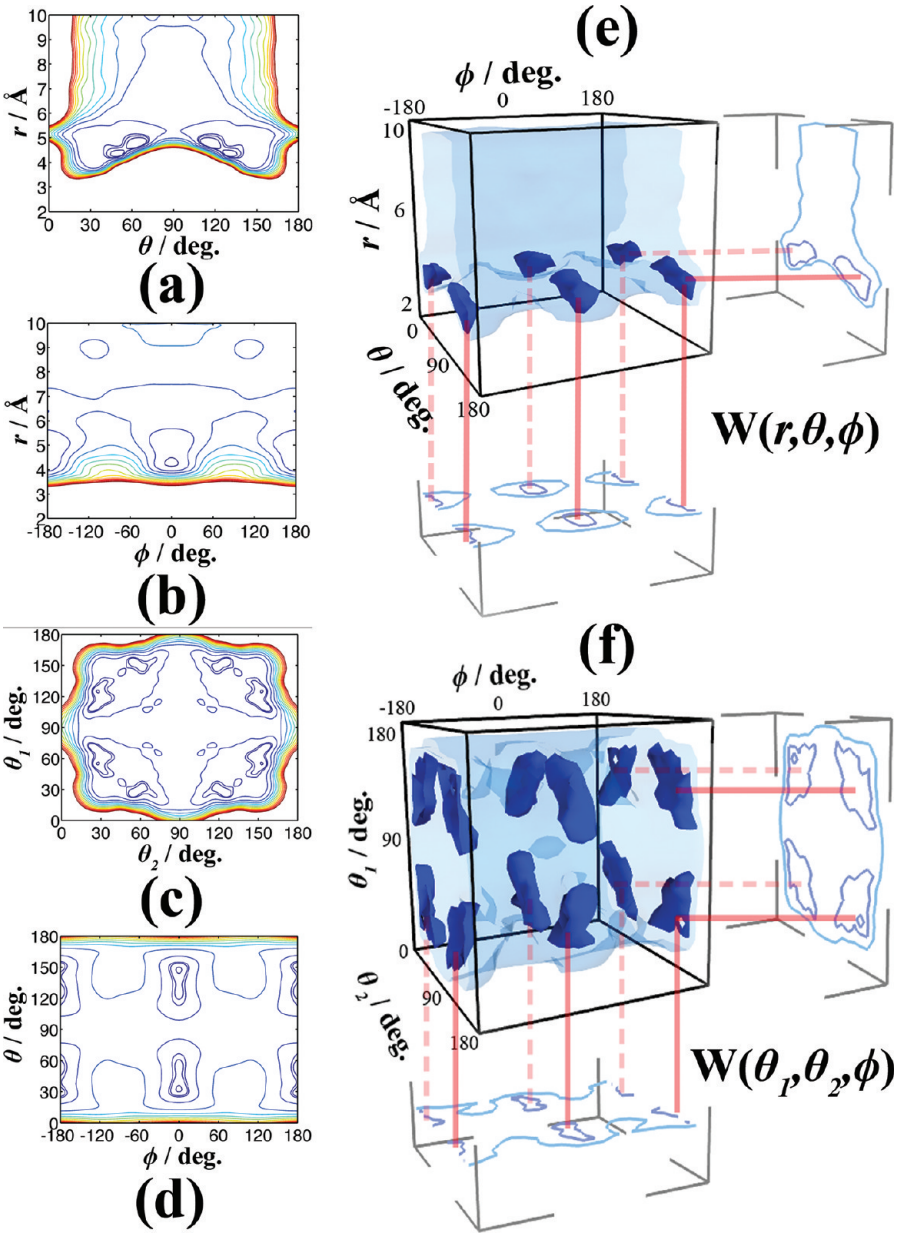

Figure 1. 2D contour (a−d) and 3D (e,f) volume plots for the benzene dimer in vacuum. The 2D contour plots are contoured at 0.5 kcal/mol from a minimum of 0.0 kcal/mol up to a maximum of 5.0 kcal/mol. The 3D volume plots have an inner contour of 1 k_BT and outer contour of 3 k_BT.

restraining potential (linear force) was applied to the edges of the distance reaction coordinate, ensuring the benzene molecules would not drift off, resulting in chemically meaningless sampling of vacuum configurational space that is far outside of the dimer electrostatic interaction field (i.e., $r > 16$ Å).

Each of the iterations consisted of eight simulations with different initial configurations and velocities. A total of 50 iterations were run. The first five iterations comprised sets of 100 ps simulations, the following 15 iterations comprised sets of 300 ps simulations, and the last 30 iterations comprised sets of 500 ps simulations. The simulation time for the entire FEARCF experiment was 160 ns (i.e., 20 ns per simulation). We used a multidimensional implementation of the weighted histogram analysis method (WHAM)[25] to combine the data from all the simulations in the set at iteration i and preceding sets from iterations $i = 1, 2, ..., n$ to obtain the free energy hypersurfaces. The data are weighted using free energy weighting factors (f_i) described previously.[14] The WHAM equations are applied iteratively until the maximum difference (tolerance) between the previous and current iteration weighting coefficients ($\max|f_j^i - f_j^{i-1}|$) is less than 0.001. The accuracy of the free energy surface is a factor of 100 less accurate than the tolerance chosen.[26] We are therefore able to distinguish between free energies that are 0.1 kcal/mol apart.

The solution FEARCF simulations were performed using the TIP4P-Ew[27] water model in a periodic cubic box of length 34.1 Å. Each simulation was run using an NVT ensemble with a constant temperature of 298.15 K, using the Nose−Hoover thermostat[28,29] and leapfrog integrator algorithm.[30,31] Here, we use double the number of simulations per iteration compared with the vacuum case (i.e., 16 simulations). Each of the simulations was initiated

with a unique dimer configuration and complement of molecular velocities in the simulation box. A total of 30 iterations was required to reach convergence. The first 3 iterations comprised simulations 100 ps in length, the next 17 iterations comprised simulations 300 ps in length, and the last 10 iterations comprised simulations of 500 ps in length. This translated into a total of 160 ns (10 ns per simulation). The WHAM[25] procedure was used to combine the data from the various simulations as described above. Unlike the vacuum experiment, no harmonic potential was used to bind the distance component of the reaction coordinate because this led to an artificial periodic sampling. The particle mesh Ewald method[32,33] was used to estimate the long-range interactions, with a grid size of 36 × 36 × 36 and a kappa value of 0.34 with a sixth order B-spline.

REDUCING THE DIMENSIONALITY OF THE FREE ENERGY VOLUME

Boltzmann-averaged 2D surface plots were calculated for $W(r, \theta_1)$ and $W(r, \phi)$ where $r \leq 10.0$ Å, and $W(\theta_1, \phi)$ and $W(\theta_1, \theta_2)$ where $r \leq 6.5$ Å were taken over the respective remaining parameters (θ_2, ϕ), (θ_1, θ_2), (r, θ_2), and (r, ϕ) from the four-dimensional $W(r, \theta_1,\theta_2, \phi)$ volumes. It must be noted that in some instances, there is a significant loss of information when reducing the dimensionality of the free energy surfaces. This has been recently illustrated for the reduction of three-, to two-, and then to one-dimensional ring pucker free energy surfaces.[18] Unambiguous geometry assignments for molecular pairs are best made from the complete $W(r, \theta_1, \theta_2, \phi)$ free energy volume. However, in the case of dimers, a well chosen three-dimensional free energy volume can adequately provide this information. We calculated $W(r, \theta_1, \phi)$ and $W(\theta_1, \theta_2, \phi)$ where the benzene molecules were in each other's attractive field (i.e., $r \leq 6.5$ Å) by taking Boltzmann averages from the four-dimensional volume $W(r, \theta_1, \theta_2, \phi)$ over the remaining orientational parameters θ_2 and ϕ, respectively.

DECONVOLUTION OF THE ENTROPY AND ENTHALPY CONTRIBUTIONS TO FREE ENERGY

We calculate the entropy of association using a "finite difference" method.[16,17] This was done by determining the one-dimensional PMFs at three well separated temperatures. The entropy was then calculated from the free energy simulations as

$$-\Delta S = \frac{\Delta A(T + \Delta T) - \Delta A(T - \Delta T)}{2\Delta T} \quad (5)$$

The 1D PMFs were run using the same conditions as described for the four-dimensional free energy hypersurface calculation. The uncertainty in ΔS using the finite difference calculation (eq 5) is inversely proportional to ΔT, implying a larger temperature difference will yield a more precise estimate of ΔS.[34] Since we wish to know the change in the entropy of association of benzene dimers in water at 298.15 K, we take the maximum temperature difference of 20 K that satisfies a lower temperature bound that is above the maximum density temperature of water (277.15 K). The three temperature simulations were therefore carried out at 278.15, 298.15, and 318.15 K.

The change in the internal energy can be related to the enthalpy of the system and was calculated using the Helmholtz free energy equation.

$$\Delta A = \Delta E - T\Delta S \quad (6)$$

The Gibbs free energies are approximately similar to the Helmholtz free energies, as seen through the work function (i.e., pdV ~ 0, in NVT simulations).

ANALYZING THE VACUUM FREE ENERGY VOLUME

Two-dimensional free energy surfaces $W(r, \theta_1)$, $W(r, \phi)$, $W(\theta_1, \phi)$, and $W(\theta_1, \theta_2)$ for the dimer in vacuum (Figure 1 a−d, respectively) are convenient to visualize the transformation between configurational minima. When viewing three-dimensional $W(r, \theta_1, \phi)$ and $W(\theta_1, \theta_2, \phi)$ volumes (Figure 1e, f) together with the two-dimensional surfaces, a clear account of the dimer configurational free energy landscape emerges. Evident from the large inner contour volumes (Figure 1 e, f) is that a collage of BT, tilted BT and PD configurations, within 0.05 kcal/mol from each other, contribute to the large minimum energy well stretching from 3.8 to 5.8 Å (Figure 1a, b). High level ab initio studies similarly found BT and PD to be the lowest energy geometries, with <0.1 kcal/mol difference between them.[35]

Although the four-dimensional $W(r, \theta_1, \theta_2, \phi)$ description is very useful, it does suffer from some loss of configurational information due to rotations about the vectors through the C_6 axes. Therefore, we cannot definitively assign configurations derived from the free energy volumes to be AoA, AoB, or BoB. This is not a major disadvantage because Gräfenstein showed that these bond and atom alignments are close in energy for specific (PD, T, and EoE) orientational configurations.[12]

The global minimum takes on an approximate tilted PD (AoA)/BT (AoA) form (r = 4.5, θ_1 = 54/126, θ_2 = 27/153, ϕ = ±180) that is similar to the low-energy PD−til-AoB and global minimum T−til-AoB configurations found by Gräfenstein and Cremer. The global minimum found from the free energy surface is only 0.04 and 0.08 kcal/mol lower in energy than the PD (r = 4.5, θ_1 = 36/144, θ_2 = 145/35, ϕ = 0) and V-shape/cogwheel/EoE (r = 4.8,θ_1 = 54/126, θ_2 = 153/27, ϕ = ±180) configurations, respectively. The vacuum free energy relationship between the lowest energy benzene dimer configurations calculated here using a classical force field corresponds well to the findings of Gräfenstein and Cremer, who showed that all T and PD stationary points are within 0.12 kcal/mol from each other on the QSCF-DC-DFT PES.[12]

We performed an optimization starting from the PD structure and found a minimum at 3.8 Å, which corresponds to the Gräfenstein and Cremer PD−AoA configuration. The same calculation was initiated from a T configuration. This time, the T-Til-AoB was found, at 4.8 Å, and is the lowest-energy configuration, therefore agreeing with Gräfenstein and Cremer's ab initio PES results. Moreover, the free-energy-derived center-of-mass-to-center-of-mass distances are in strong agreement with those of vacuum experiments of 4.96 Å.[36] The vacuum free energy results using classical CHARMM force field parameters show a strong correlation with the minimm configurations and their relative energetic preference as found from high-level QM calculations.[11,35,37] The accuracy of the molecular mechanics potential energy function is validated because it discriminates similarly between low-energy conformers, as investigations using quantum Hamiltonians do.

The broadness of the low-energy ($\leq 1/2k_BT$) configuration well (Figure 1a−d) suggests that the mix of the PD, BT, and V

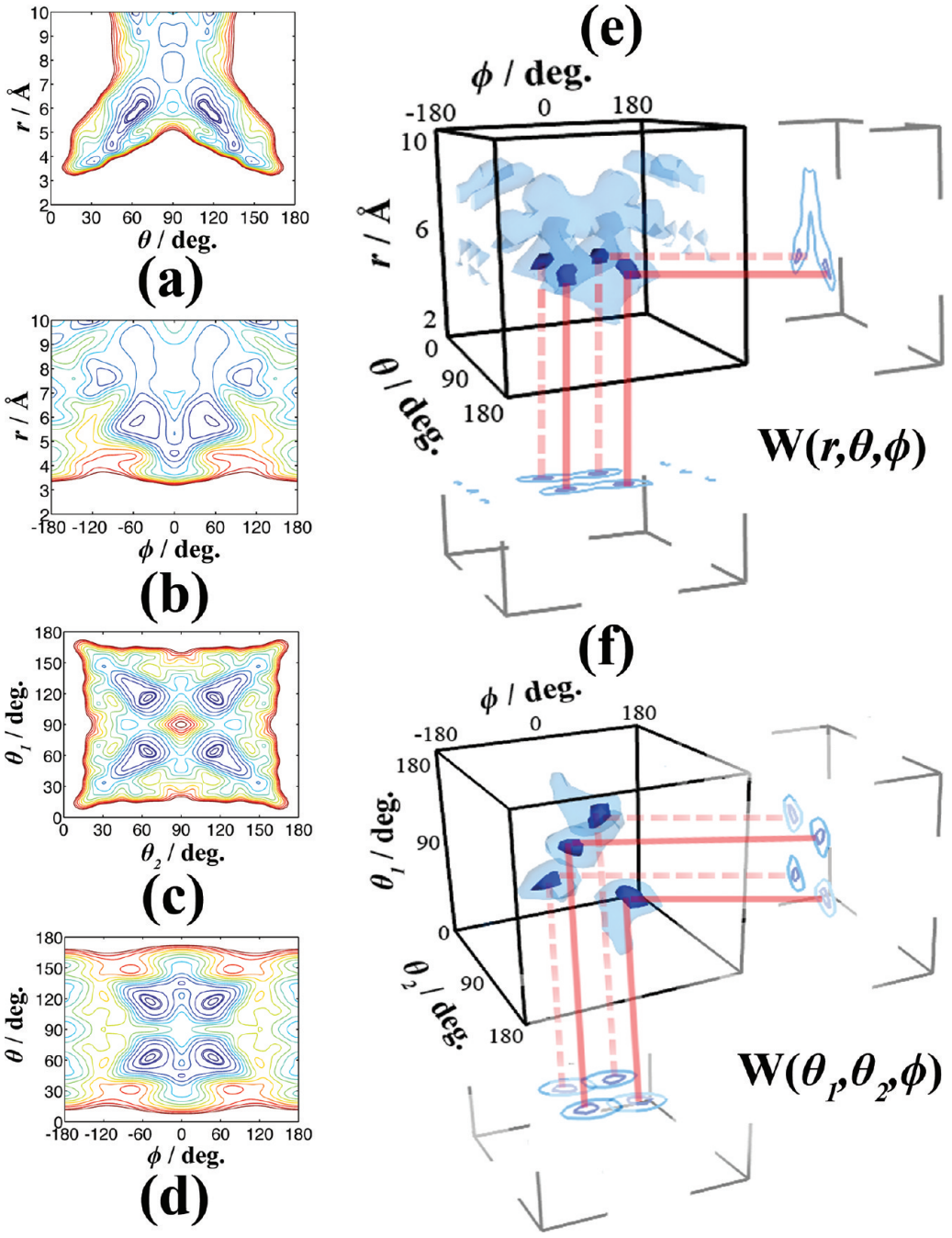

Figure 2. 2D contour (a−d) and 3D (e−f) volume plots for the benzene dimer in solution (TIP4P−Ew water). The 2D contour plots are contoured at 0.5 kcal/mol from a minimum of 0.0 kcal/mol up to a maximum of 5.0 kcal/mol. The 3D volume plots have an inner contour of 1 k_BT and outer contour of 3 k_BT.

(or EoE) are in dynamic equilibrium. From the Boltzmann averaged $W(r, \theta_1)$, $W(r, \phi)$, $W(\theta_1, \phi)$, and $W(\theta_1, \theta_2)$, surfaces it can be seen that the minima are symmetrical about $\theta = 90$ and $\phi = 0$ and that they display no significant energy barriers between canonical configurations. The basin of free energy minima (Figure 1a−d) is well within the thermal energy envelope, leading to a random ensemble of low-energy configurations in vacuum. This result opposes the notion that there are specific energetically favorable benzene dimer orientations that bias the association of these molecules, since the geometries can easily vary among the various minimum energy configurations.

The orientationally biased aromatic associations observed in protein structures[2,38] therefore cannot be explained by the nature of the potential energy surface. In an analysis of interaction energies performed on optimized couple cluster structures, Sherrill et al.[37] concluded that two closely associating benzene molecules either maximizes individual contributions from the van der Waals and electrostatic interactions or optimizes the balance between these two sources of attraction. Using symmetry-adapted perturbation theory combined with density functional theory, Podeszwa et al., showed that dispersion is the dominant contribution to the PD configuration's stability.

In the BT case, electrostatics—in particular, quadrupole—quadrupole—have been proposed to stabilize that configuration.[35] Vacuum experiments such as Raman-vibronic double resonance spectroscopy[39] and Fourier transform microwave spectroscopy[36] attempt to deconvolute very complex spectra for the dimer. These concluded that there are two inequivalent benzene sites suggestive of T-shape-type structures. The free energy volumes for the vacuum benzene dimer shown here reveal more T and T-like structures than parallel or stacked structures in the low energy basins. The experimental observation that there is much uncertainty in the dimer configurations along with the very minor differences in the dispersion and electrostatic terms derived from computed couple cluster methods[40] correlates well with the ensemble of PD, BT, and V/CGW (or EoE) configurations observed from the free energy vacuum simulations. Our results suggest a 2:1 stoichiometeric ratio between T (and T-like) and PD configurations. This may possibly explain the discrepancy between experiment and high-level static quantum mechanical calculations.

ANALYZING THE SOLUTION FREE ENERGY VOLUME

In solution, unlike in vacuum, the thermodynamically distinct low-energy geometries are separated by at least 1 k_BT from each other, as can be seen from the ~0.59 kcal/mol contour volumes colored in dark blue (Figure 2e, f). These are well-defined low-energy regions that are far smaller and fewer in number compared with the vacuum case contoured at the same energy levels (Figure 1e, f). The global minimum symmetrical configurations (r = 5.8, θ_1 = 63/117, θ_2 = 117/63, ϕ = −53) and (r = 5.8, θ_1 = 63/117, θ_2 = 63/117, ϕ = 53) observed from the $W(r, \theta_1)$, $W(r, \phi)$, $W(\theta_1, \phi)$, and $W(\theta_1, \theta_2)$ 2D free energy surfaces correspond to Gräfenstein and Cremer's EoE definition.[12] They found this configuration to be nearly 1 kcal/mol higher in energy on their PES than the global minimum. The EoE configuration is similar in form to the cogwheel (CW) structures observed by Thornton et al., which is the predominantly observed configuration for phenylalanine dimers in proteins.[38]

The PD−tilted-AoB (r = 5.8, θ_1 = 45/135, θ_2 = 45/135, ϕ = 0) configurations are 0.45 kcal/mol higher in energy than the global minimum on the solution free energy surface. Nonetheless, the PD−tilted-AoB and EoE configurations are separated from each other by less than 1 k_BT, allowing for regular interconversion between them. As the benzene molecules move out of each other's potential energy field, where specific PD−tilted-AoB and EoE configurations are favored, a solvent shared minimum appears at r = 7.5 Å. This minimum found at larger benzene separations has been observed by others as a very weak minima in 1D $W(r)$ PMFs.[10,11] The orientational preference for the two benzene molecules at this distance is an SbS arrangement, which could be interpreted as an elongated EoE configuration. The competing attractive forces among water, water and benzene, and the benzene molecules result in the formation of a solvent shared minimum. This phenomenon is predominantly found in charge systems[41] but has been found by others for the benzene dimer.[8,10,11] We find that the SbS minima is 1.29 kcal/mol higher in energy than the close contact global minimum configuration found at r = 5.8. Although these configurations are energetically distinct from each other (Figure 2), the energy barriers separating them are less than 3 k_BT and should result in rapid and frequent interconversion between EoE, PD−tilted-AoB, BT−AoA, PD−AoA, and SbS configurations. The BT, V-shape/cogwheel, and SbS arrangements that appear have been conjectured from six-dimensional deconvolution calculations performed on neutron diffraction benzene solvent structure factor data.[42] Although the energy barriers separating dimer configurations are more than 3-fold greater in water (<1.78 kcal/mol) than they are in vacuum (<0.58 kcal/mol), they remain very low and would make the observation of specific dimer configurations experimentally very difficult.

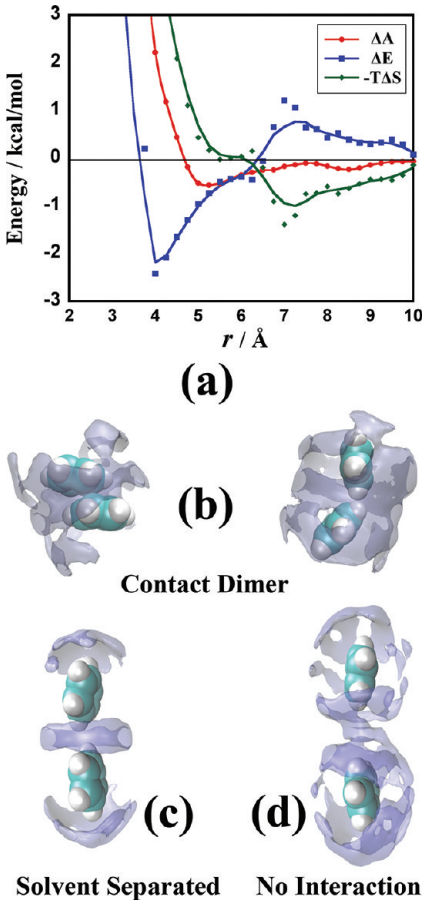

Figure 3. The thermodynamic curves (a) and water probability density (b−d) profiles for the benzene dimer.

ENTROPY OF ASSOCIATION DETERMINES ORIENTATION

The interaction in vacuum is mainly driven by a large enthalpic contribution to the free energy, as found by Podeszwa et al.[35] from their potential energy surface of the benzene dimer obtained using symmetry adapted perturbation theory (SAPT). The thermodynamic data for the solution case (i.e., the change in free energy ΔA, internal energy ΔE, and entropy ΔS) is shown in Figure 3a. To obtain the thermodynamic data, three PMFs were 1calculated as a function of the distance between the benzenes centers of mass at 278.15, 298.15, and 318.15 K. The 1D distance PMF reveals a global minimum at a separation of r = 5.8 Å, which is consistent with previous studies[10,11,43] and with the multidimensional anisotropic free energy of association PMFs shown in Figure 2. The thermodynamic analysis shows that the major contribution to the contact (r = 5.5 Å) EoE dimer configuration (along with the PD and BT configurations) is enthalpic (blue curve).

dx.doi.org/10.1021/jp2077159 |J. Phys. Chem. B 2012, 116, 324–331

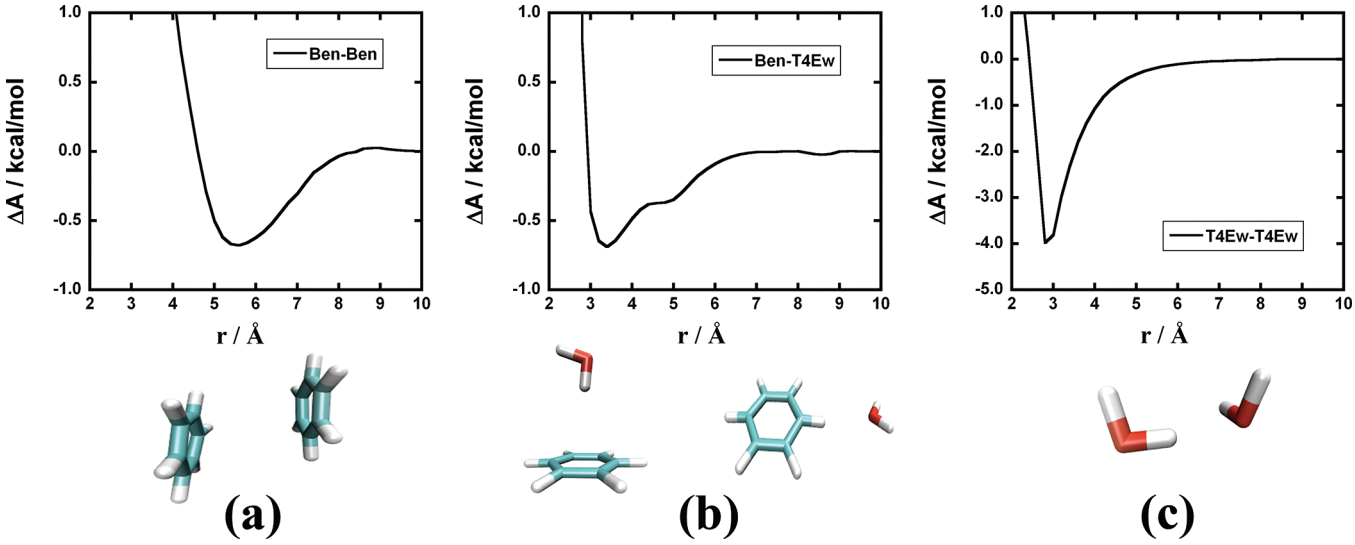

Figure 4. The various interactions between (a) benzene−benzene, (b) benzene−water and (c) water−water molecules, in vacuum.

However, the location of the global free energy minimum is not at the lowest attractive energy point at 4.0 Å (blue curve), but is closer to the local entropy minimum at 5.5 Å (green curve).

The broad appearance of the $W(r)$ global minimum well indicates that several configurations are contributing to it. This is verified by the 2D surfaces and 3D volumes (Figure 2) for which the nature of the contributing structures have been described above. Minor but important points of inflection are observed for both the entropy and energy curves at a distance of ∼6.0 Å. These suggest that the dominance of enthalpically prescribed contact dimer configurations diminishes compared with the entropically favored solvent-shared configuration that more influences the relative orientation of the benzenes on close association. It may therefore seem that this is the critical distance at which a close contact benzene dimer in solution may be defined. This suggests that the entropy (of associating benzenes in solution) determines the separation distance and orientation of benzene dimer association in solution.

A comparison of the 1D vacuum PMFs for the benzene dimer, benzene-water and the water dimer (Figure 4) reveals that the free energy of association of benzene−water is weaker than that of the benzene dimer at 6.0 Å; however, the former is dominant at distances <4.0 Å. As the benzene molecules approach each other, the characteristics of the solvent-separated minimum configuration remain; there is, however, a decrease in water probability around the dimer, that is, a decrease in density of fixed water configurations. This corresponds to an increase in association entropy, that is, a minimum in the $-T\Delta S$ curve. The benzenes therefore experience greater tumbling motion in the EoE configuration. This leads to a decrease in water probability, suggesting that bound waters are released.

CONCLUSION

There is large variation in the configurations that contribute to the free energy minimum wells of the vacuum benzene contact pair, compared with far fewer and more energetically distinct solution close contact benzene dimer configurations. The EoE configuration is most probable in solution and appears to evolve from the entropically favored SbS solvent shared configuration. Benzene association in water therefore optimizes three effects: (1) the increase in the entropic gain due to bound waters that are released from benzene molecules on their association, (2) the freedom of the benzenes to rotate, and (3) the potential energy gain from the attraction between the benzene molecules. Although the association of the benzene dimer is accepted to be the result of the hydrophobic effect, the relative orientation of the benzene molecules is a result of maximizing the contribution that the benzene−benzene entropy of association makes to the total solution free energy.

AUTHOR INFORMATION

Corresponding Author

*Fax: +2721 686 4333. E-mail: kevin.naidoo@uct.ac.za.

ACKNOWLEDGMENT

This work is based upon research supported by the South African Research Chairs Initiative (SARChI) of the Department of Science and Technology and National Research Foundation awarded to K.J.N. M.R.G. thanks SARChI and the National Research Foundation (Pretoria) for a doctoral fellowship/support. J.S. thanks the National Research Foundation (Pretoria) for a M.Sc. fellowship.

REFERENCES

(1) Schliwa, M.; Woehlke, G. *Nature* **2003**, *422*, 759.
(2) Burley, S. K.; Petsko, G. A. *Science* **1985**, *229*, 23.
(3) McGaughey, G. B.; Gagne, M.; Rappe, A. K. *J. Biol. Chem.* **1998**, *273*, 15458.
(4) Bhattacharyya, R.; Samanta, U.; Chakrabarti, P. *Protein Eng.* **2002**, *15*, 91.
(5) Strickland-Constable, R. F. *Kinetics and Mechanism of Crystallization from the Fluid Phase and of the Condensation and Evaporation of Liquids*; Academic Press: London, 1968.
(6) Collings, P. J. *Liquid Crystals: Nature's Delicate Phase of Matter*; Princeton University Press: Princeton, 1990.
(7) Cockroft, S. L.; Hunter, C. A.; Lawson, K. R.; Perkins, J.; Urch, C. J. *J. Am. Chem. Soc.* **2005**, *127*, 8594.
(8) Linse, P. *J. Am. Chem. Soc.* **1992**, *114*, 4366.
(9) Sinnokrot, M. O.; Sherrill, C. D. *J. Phys. Chem. A* **2006**, *110*, 10656.

(10) Jorgensen, W. L.; Severance, D. L. *J. Am. Chem. Soc.* **1990**, *112*, 4768.
(11) Chipot, C.; Jaffe, R.; Maigret, B.; Pearlman, D. A.; Kollman, P. A. *J. Am. Chem. Soc.* **1996**, *118*, 11217.
(12) Grafenstein, J.; Cremer, D. *J. Chem. Phys.* **2009**, *130*, 16.
(13) Brooks, B. R.; Bruccoleri, R. E.; Olafson, B. D.; States, D. J.; Swaminathan, S.; Karplus, M. *J. Comput. Chem.* **1983**, *4* (2), 187.
(14) Strümpfer, J.; Naidoo, K. J. *J. Comput. Chem.* **2010**, *31*, 308.
(15) Barnett, C. B.; Naidoo, K. J. *Mol. Phys.* **2009**, *107*, 1243.
(16) Smith, D. E.; Zhang, L.; Haymet, A. D. J. *J. Am. Chem. Soc.* **1992**, *114*, 5875.
(17) Smith, P. E.; Van Gunsteren, W. F. *J. Chem. Phys.* **1993**, *100*, 575.
(18) Barnett, C. B.; Naidoo, K. J. *J. Phys. Chem. B* **2010**, *114*, 17142.
(19) Naidoo, K. J. *Chem. Sci. Chin.* **2011**, *54*, 1.
(20) Berkowitz, M.; Karim, O. A.; McCammon, J. A.; Rossky, P. J. *Chem. Phys. Lett.* **1984**, *105*, 577.
(21) Belch, A. C.; Berkowitz, M.; McCammon, J. A. *J. Am. Chem. Soc.* **1986**, *108*, 1755.
(22) Trzesniak, D.; Kunz, A. P. E.; van Gunsteren, W. F. *ChemPhysChem* **2007**, *8*, 162.
(23) Khavrutskii, I. V.; Dzubiella, J.; McCammon, J. A. *J. Chem. Phys.* **2008**, *128*, 044106.
(24) Lamoureux, G.; Roux, B. *J. Chem. Phys.* **2003**, *119*, 3025.
(25) Kumar, S.; Rosenberg, J. M.; Bouzida, D.; Swendsen, R. H.; Kollman, P. A. *J. Comput. Chem.* **1995**, *16*, 1339.
(26) Ghosh, I.; McCammon, J. A. *Biophys. J.* **1987**, *51*, 637.
(27) Horn, H. W.; Swope, W. C.; Pitera, J. W.; Madura, J. D.; Dick, T. J.; Hura, G. L.; Head-Gordon, T. *J. Chem. Phys.* **2004**, *120*, 9665.
(28) Nose, S. *Mol. Phys.* **1984**, *52*, 255.
(29) Hoover, W. G. *Phys. Rev. A* **1985**, *31*, 1695.
(30) Hockney, R. W.; Eastwood, J. W. *Computer Simulations Using Particles*; McGraw-Hill: New York, 1981.
(31) Amini, M.; Eastwood, J. W.; Hockney, R. W. *Comput. Phys. Commun.* **1987**, *44*, 83.
(32) York, D. M.; Darden, T. A.; Pedersen, L. G. *J. Chem. Phys.* **1993**, *99*, 8345.
(33) Essmann, U.; Perera, L.; Berkowitz, M. L.; Darden, T.; Lee, H.; Pedersen, L. G. *J. Chem. Phys.* **1995**, *103*, 8577.
(34) Smith, D. E.; Haymet, A. D. J. *J. Chem. Phys.* **1993**, *98*, 6445.
(35) Podeszwa, R.; Bukowski, R.; Szalewicz, K. *J. Phys. Chem. A* **2006**, *110*, 10345.
(36) Arunan, E.; Gutowsky, H. S. *J. Chem. Phys.* **1993**, *98*, 4294.
(37) Sherrill, C. D.; Takatani, T.; Hohenstein, E. G. *J. Phys. Chem. A* **2009**, *113*, 10146.
(38) Singh, J.; Thornton, J. M. *FEBS Lett.* **1985**, *191*, 1.
(39) Henson, B. F.; Hartland, G. V.; Venturo, V. A.; Felker, P. M. *J. Chem. Phys.* **1992**, *97*, 2189.
(40) Tsuzuki, S.; Honda, K.; Uchimaru, T.; Mikami, M.; Tanabe, K. *J. Am. Chem. Soc.* **2002**, *124*, 104.
(41) Matthews, R. P.; Naidoo, K. J. *J. Phys. Chem. B* **2010**, *114*, 7286.
(42) Headen, T. F.; Howard, C. A.; Skipper, N. T.; Wilkinson, M. A.; Bowron, D. T.; Soper, A. K. *J. Am. Chem. Soc.* **2010**, *132*, 5735.
(43) Gao, J. *J. Am. Chem. Soc.* **1993**, *115*, 6893.